AIAA JOURNAL
Vol. 33, No. 4, April 1995

Stress Considerations in Reduced-Size Aeroelastic Optimization

M. Karpel* and L. Brainin†
Technion—Israel Institute of Technology, Haifa 32000, Israel

The modal approach, which is normally used in analysis and optimization with dynamic aeroelastic considerations, is extended here to deal with static aeroelastic maneuver trim equations, loads, and stresses. Reduced-size static equilibrium equations, where a subset of low-frequency vibration modes of a baseline structure is used as generalized coordinates, are formulated such that they can be used for modified structures without changing the coordinates. These expressions and their derivatives with respect to structural design variables are investigated in comparison with full-size finite element solutions. A new method, which uses modal stress perturbations of the baseline structure to predict stresses in the modified ones, is developed. The modal perturbation approach facilitates high-accuracy computations of stress sensitivities without increasing the model size. The presented formulation facilitates an efficient inclusion of stress and load considerations in on-line aeroservoelastic optimal design schemes.

Introduction

THE structural design of flight vehicles requires an integrated approach in which various aeroelastic aspects such as flutter margins, control effectiveness, interaction with the control system, static and dynamic loads, and structural stresses are considered. Common design processes start with the definition of a preliminary set of design loads and the construction of an initial finite element model that satisfies basic stress and buckling requirements. This model is then used for the various aeroelastic analyses in several design cycles. The possibly strong and contradicting effects of design changes on the various disciplines imply that the design process can be more efficient if different aspects are considered simultaneously in an automated optimized process.

For the sake of numerical efficiency, it is desired to formulate the various analyses such that the repetitive computations are performed with reduced-size models and are using a common data base. However, even though the different analyses can be based on the same finite element model, the common solutions involve matrix equations of substantially different types and sizes. Although stress analysis, for example, normally requires the full detailed discrete-coordinate stiffness matrix of typically thousands degrees of freedom, flutter analysis is usually based on about 10 modal coordinates. Consequently, several integrated aeroelastic optimization processes that included static and dynamic considerations, such as those of Refs. 1–4, used full discrete-coordinate physical models for the static considerations and reduced-size modal models for the dynamic ones.[5]

Some techniques were recently developed in order to reduce the problem size in repetitive stress calculations during integrated optimization. Livne et al.[6] used the equivalent plate approach of Giles,[7] which requires special modeling efforts and might not correspond to actual structures as well as standard finite element models do. Bindolino et al.[8] used the perturbation mode approach[9] in which the displacements due to each loading case are linear combinations of the baseline displacement vector and its derivatives with respect to the design variables. The problem size in this case is proportional to the number of design variables. The application of Ref. 8 showed efficient and accurate solution in optimization with one design load case. This approach, however, does not take into account load redistribution due to structural changes and may become inefficient in optimization with multiple loading cases.

Received March 21, 1994; presented as Paper 94-1480 at the AIAA 35th Structures, Structural Dynamics, and Materials Conference, Hilton Head, SC, April 18–20, 1994; revision received Sept. 28, 1994; accepted for publication Sept. 28, 1994.

*Associate Professor, Department of Aerospace Engineering. Member AIAA.

†Graduate Student, Department of Aerospace Engineering.

The approach taken in Refs. 10 and 11 was to extend the modal-coordinate formulation to deal with static aeroelastic analysis and optimization. The basic assumption of the modal approach is that the elastic deflections and rigid-body movements of a flight vehicle can be represented as a linear combination of a limited set of predefined deflection modes. Under this assumption, the equations of motion are transformed from physical coordinates to new modal coordinates. The limited number of the modes taken into account results in reduced-size analysis matrices, thus inherently contributing to the efficiency of the analysis. The modes in Refs. 10 and 11, and in this work, are a relatively small set of low-frequency free-free normal vibration modes of the vehicle, including rigid-body modes. Applications to the wing design of a fighter aircraft, with divergence and control effectiveness considerations, showed small errors compared to full finite element solutions. Although flutter required 10–20 modes in this application, static aeroelasticity required 20–30 modes, which still reduced the computational efforts by orders of magnitude, compared to the full solutions.

The modal approach was included in the modal-based multidisciplinary optimization scheme of Ref. 12 (which dealt with flutter, control margins, and aeroelastic effectiveness) and showed excellent accuracy in applications to the composite active flexible wing (AFW) model, which has four control surfaces. The fact that all disciplines were based on the same modal coordinates, had analytical sensitivities to the design variables, and used a common data base yielded an integrated optimization process that was performed in several minutes on a workstation. Continuous-gust response considerations were added later with minor effect on computation efficiency.[13] It is desired to add stress considerations to this scheme, including aeroelastic effects of structural changes on load distributions.

The problem of stress accuracy with the modal approach is quite old. Bisplinghoff et al.[5] described two methods for calculating modal-based stresses, the mode displacement (MD) and the mode acceleration (MA) method. MD stresses are calculated directly from the modal displacements. Since stresses are the result of displacement differentiation, small modal truncation errors may cause large stress errors. The MA approach uses the modal acceleration response to calculate the inertial loads and add them to the excitation forces. Stresses are calculated from the MA loads with the full-size model. Expressions for derivatives of transient modal acceleration response with respect to structural design variables are given by Haftka et al.[14] When aeroelastic loads are added, the MA method becomes the summation-of-forces (SOF) method. Sensitivity analysis of SOF loads with application to transport aircraft was presented by D'Vari and Baker.[15]

The return to the full finite element model in each optimization step requires large computational efforts. One purpose of this paper is to show that MD analysis can also yield high-accuracy stresses, at least in simple wing design cases, with a reasonable number

of low-frequency modes taken into account. The main purpose is to present a new modal perturbation method for calculating high-accuracy stresses of modified structures, and their derivatives with respect to the design variables, with the modal data base of the baseline structure. It will be shown that the computational efforts in including stress considerations in modal-based multidisciplinary optimization can be reduced very significantly. For the sake of clarity and completeness, the analytical developments include well-known aeroelastic trim, load, and stress equations formulated in a way that supports the presentation of the new method and helps to explain the optimization procedure and the numerical examples.

Aeroelastic Trim

The discrete-coordinate equation of motion of the aeroelastic system reads

$$[M]\{\ddot{u}\} + [C]\{\dot{u}\} + [K]\{u\} = \{F_A\} + \{F_0\} \tag{1}$$

where $\{u\}$ is the vector of structural displacements; $[M]$, $[C]$, and $[K]$ are the mass, damping, and stiffness matrices of order n; $\{F_0\}$ is the vector of external forces acting on the vehicle at a reference "zero" position; and $\{F_A\}$ is the vector of aerodynamic forces due rigid-body and elastic motion, and control surface deflections, relative to the reference position. With linear, quasisteady aerodynamics, $\{F_A\}$ is expressed by

$$\{F_A\} = q[T_{AS}]^T[AFC] \times \left([T_{\alpha S}](\{u\} + [\phi_C]\{\xi_C\}) - \frac{1}{V}[T_{CS}]\{\dot{u}\} \right) \tag{2}$$

where $[AFC]$ is the steady aerodynamic force-coefficient matrix defined by a linear panel method, q is the dynamic pressure, and V is the true aircraft velocity. Here, $[\phi_C]$ is a matrix of control surface deflection modes, defined by kinematic deflections of control surfaces with zeros elsewhere, and $\{\xi_C\}$ is a vector of control commands. The terms $[T_{AS}]$, $[T_{\alpha S}]$, and $[T_{CS}]$ are transformation matrices from deflections in the structural grid to deflections at the panel pressure centers, pitch rotations at the panel control points (at which local angles of attack are defined), and deflections at the panel control points.

The basic assumption in the modal approach is that the structural deflections can be adequately defined as

$$\{u\} = [\phi_R]\{\xi_R\} + [\phi_E]\{\xi_E\} \tag{3}$$

where $[\phi_R]$ and $[\phi_E]$ are matrices of rigid and elastic natural vibration modes of the baseline structure. Even though the mass and stiffness matrices are changed during the optimization process used in this work, the modes that serve as generalized coordinates remain unchanged. The validity of Eq. (3), which depends on the number n_m and type of modes included in $[\phi_E]$ and on the structural changes, is discussed in the following sections. For the sake of computation efficiency, it is desired to use Eq. (3) with $n_m \ll n$.

The substitution of Eqs. (2) and (3) in Eq. (1), premultiplication by $[\phi_R\ \phi_E]^T$, and the quasisteady assumption that terms associated with $\{\ddot{\xi}_E\}$ and $\{\dot{\xi}_E\}$ are negligible yield

$$\begin{bmatrix} M_{RR} \\ M_{ER} \end{bmatrix}\{\ddot{\xi}_R\} + \begin{bmatrix} 0 & 0 \\ 0 & K_{EE} \end{bmatrix}\begin{Bmatrix} \xi_R \\ \xi_E \end{Bmatrix} = q\begin{bmatrix} Q_{RR} & Q_{RE} \\ Q_{ER} & Q_{EE} \end{bmatrix} \times \begin{Bmatrix} \xi_R \\ \xi_E \end{Bmatrix} + \frac{q}{V}\begin{bmatrix} Q_{R\dot{R}} \\ Q_{E\dot{R}} \end{bmatrix}\{\dot{\xi}_R\} + q\begin{bmatrix} Q_{RC} \\ Q_{EC} \end{bmatrix}\{\xi_C\} + \begin{bmatrix} \phi_R^T \\ \phi_E^T \end{bmatrix}\{F_0\} \tag{4}$$

where the generalised aerodynamic matrices are

$$\begin{bmatrix} Q_{RR} & Q_{RE} & Q_{R\dot{R}} & Q_{RC} \\ Q_{ER} & Q_{EE} & Q_{E\dot{R}} & Q_{EC} \end{bmatrix} = \begin{bmatrix} \phi_R^T \\ \phi_E^T \end{bmatrix}[T_{AS}]^T[AFC] \times \left[[T_{\alpha S}][\phi_R] \quad [T_{\alpha S}][\phi_E] \quad -[T_{CS}][\phi_R] \quad [T_{\alpha S}][\phi_C] \right]$$

and the generalized mass and stiffness matrices are

$$\begin{bmatrix} M_{RR} \\ M_{ER} \end{bmatrix} = \begin{bmatrix} \phi_R^T \\ \phi_E^T \end{bmatrix}[M][\phi_R] \tag{5}$$

$$[K_{EE}] = [\phi_E]^T[K][\phi_E] \tag{6}$$

Due to mode orthogonality, $[K_{EE}]$ is diagonal and $[M_{ER}] = 0$ in the baseline structure, but not in a modified one. The $[M_{ER}]$ term was neglected in the formulation of Refs. 11 and 12, where the only static aeroelastic issue was control effectiveness.

The second row of Eq. (4) can be used to extract the modal elastic deflections

$$\{\xi_E\} = [D]\{X_R\} + [B][\phi_E]^T\{F_0\} \tag{7}$$

where

$$[B] = ([K_{EE}] - q[Q_{EE}])^{-1}$$

$$[D] = [B]\left[qQ_{ER} \quad \frac{q}{V}Q_{E\dot{R}} \quad -M_{ER} \quad qQ_{EC} \right]$$

and $\{X_R\}$ is the vector of the aircraft rigid-body displacements, velocities, and accelerations (linear and angular) and control surface deflections

$$\{X_R\}^T = \left[\xi_R^T \quad \dot{\xi}_R^T \quad \ddot{\xi}_R^T \quad \xi_C^T \right] \tag{8}$$

The substitution of Eq. (7) in Eq. (4) yields the quasisteady maneuver trim equation

$$[A]\{X_R\} = \{\tilde{F}_0\} \tag{9}$$

where

$$[A] = -\left[qQ_{RR} \quad \frac{q}{V}Q_{R\dot{R}} \quad -M_{RR} \quad qQ_{RC} \right] - q[Q_{RE}][D]$$

$$\{\tilde{F}_0\} = \left[[\phi_R]^T + q[Q_{RE}][B][\phi_E]^T \right]\{F_0\}$$

Equation (9) reflects an underdetermined system of n_R equations with $3n_R + n_C$ unknowns. In order to define a particular maneuver, one has to define $2n_R + n_C$ variables and solve Eq. (9) for the remaining n_R free variables, as demonstrated in the numerical example. The definition of the $2n_R + n_C$ variables may require a solution of the kinematic equations that define the maneuver. The aerodynamic parts in $[A]$ are integral stability and control coefficients with aeroelastic effects. Their division by the respective "rigid" coefficients gives the associated aeroelastic effectiveness coefficients.

The optimization process starts with the definition of n_p structural design variables, where each variable is a geometric property (such as thickness or cross-sectional area) of a group of finite elements. It is assumed in this work that the mass and stiffness matrices are linear with the design variables. Hence, the derivatives of the generalized mass and stiffness matrices with respect to a design variable p_k can be calculated for the baseline structure by Eqs. (5) and (6), with $[M]$ and $[K]$ replaced by $\partial[M]/\partial p_k$ and $\partial[K]/\partial p_k$. The resulting $\partial[M_{RR}]/\partial p_k$, $\partial[M_{ER}]/\partial p_k$, and $\partial[K_{EE}]/\partial p_k$ are saved in the data base. The linearity assumption is adequate for most design variables commonly used for structural wing design,[3] such as the thickness of thin-skin elements, the width of spar webs, and the area of spar caps and stringers. Cubic expressions, to be used, for example, when bending effects in plate elements are significant, are discussed in Ref. 13. The inclusion of such elements would require additional coefficient matrices to be stored in the data base without causing significant computational effects.

The updated generalized matrices throughout the optimization process are calculated by

$$\begin{bmatrix} \bar{M}_{RR} \\ \bar{M}_{ER} \end{bmatrix} = \begin{bmatrix} M_{RR} \\ 0 \end{bmatrix} + \sum_{k=1}^{n_p} \Delta p_k \frac{\partial}{\partial p_k}\begin{bmatrix} M_{RR} \\ M_{ER} \end{bmatrix} \tag{10}$$

$$[\bar{K}_{EE}] = [K_{EE}] + \sum_{k=1}^{n_p} \Delta p_k \frac{\partial [K_{EE}]}{\partial p_k} \tag{11}$$

To find the trim variables and the elastic deformations of a modified structure, Eqs. (7) and (9) are used with $[B]$, $[D]$, and $[A]$ replaced by $[\bar{B}]$, $[\bar{D}]$, and $[\bar{A}]$, where the generalized matrices are replaced by those of Eqs. (10) and (11).

The differentiation of Eq. (9) with respect to p_k, using

$$\frac{\partial[\bar{B}]}{\partial p_k} = -[\bar{B}]\frac{\partial[K_{EE}]}{\partial p_k}[\bar{B}] \tag{12}$$

yields the underdetermined expression for the sensitivities of the trim variables

$$[\bar{A}]\frac{\partial\{X_R\}}{\partial p_k} = -\left(\frac{\partial[M_{RR}]}{\partial p_k} + q[Q_{RE}][\bar{B}]\frac{\partial[M_{ER}]}{\partial p_k}\right)\{\ddot{\xi}_R\}$$

$$- q[Q_{RE}][\bar{B}]\frac{\partial[K_{EE}]}{\partial p_k}\left([\bar{D}]\{X_R\} + [\bar{B}][\phi_E]^T\{F_0\}\right) \tag{13}$$

The derivatives of the $2n_R + n_C$ variables that were fixed by the defined maneuver in Eq. (9) are set to zero, and Eq. (13) is then solved for the sensitivities of the n_R free trim variables. The differentiation of Eq. (7) yields the sensitivities of the modal displacements

$$\frac{\partial\{\xi_E\}}{\partial p_k} = -[\bar{B}]\left(\frac{\partial[K_{EE}]}{\partial p_k}\{\xi_E\} + \frac{\partial[M_{ER}]}{\partial p_k}\{\ddot{\xi}_R\}\right) + [\bar{D}]\frac{\partial\{X_R\}}{\partial p_k} \tag{14}$$

which will be used for sensitivities of loads and stresses in the following sections.

Design Loads

The design loads in this paper are based on quasisteady trim with linear aerodynamics. Applications of the modal approach to dynamic loads are discussed in Ref. 13 for continuous-gust loads and in Ref. 16 for impulsive excitation loads. The trim solution of Eq. (9) and the modal deformations of Eq. (7) define the structural displacements needed for the calculation of the net loads associated with a defined maneuver. The net load vector $\{F_{\text{net}}\}$ can be calculated by either the SOF method

$$\{F_{\text{sof}}\} = \{F_A\} + \{F_0\} - [\bar{M}][\phi_R]\{\ddot{\xi}_R\} \tag{15}$$

where $\{F_A\}$ is calculated by Eq. (2), or by the MD method

$$\{F_{\text{md}}\} = [\bar{K}][\phi_E]\{\xi_E\} \tag{16}$$

As deduced from Eq. (1), with damping forces neglected, and from Eq. (3), the two vectors are effectively identical when the modal assumption is valid.[16]

Integrated section loads, which are often used to characterize the load cases, are related to $\{F_{\text{net}}\}$ of either Eq. (15) or (16) by

$$\{L\} = [\phi_L]^T\{F_{\text{net}}\} \tag{17}$$

where $[\phi_L]$ is a matrix of kinematic integration vectors called *load modes*. An efficient way to generate the load modes together with the baseline vibration modes is given in Ref. 16. It is also shown in Ref. 16 that section loads can be expressed in terms of the trim variables, the modal deformations and the generalized aerodynamic and mass matrices, without the need to calculate $\{F_{\text{net}}\}$ explicitly.

The SOF section-load sensitivities are obtained by the differentiation of Eq. (17) using Eqs. (2), (3), and (15), which yields

$$\frac{\partial\{L_{\text{sof}}\}}{\partial p_k} = -\frac{\partial[M_{LR}]}{\partial p_k}\{\ddot{\xi}_R\} - [\bar{M}_{LR}]\frac{\partial\{\ddot{\xi}_R\}}{\partial p_k} + q[Q_{LR}]\frac{\partial\{\xi_R\}}{\partial p_k}$$

$$+ q[Q_{LE}]\frac{\partial\{\xi_E\}}{\partial p_k} + q[Q_{LC}]\frac{\partial\{\xi_C\}}{\partial p_k} + \frac{q}{V}[Q_{L\dot{R}}]\frac{\partial\{\dot{\xi}_R\}}{\partial p_k} \tag{18}$$

where the coefficient matrices are similar to those of Eqs. (4), (5), and (10), but calculated with left multiplication by $[\phi_L^T]$. Equation (18) is based on the trim variables, their sensitivities [Eq. (13)], and the sensitivities of the modal deflections [Eq. (14)]. The MD section-load sensitivities are obtained by differentiation of Eq. (17) using Eq. (16), which yields

$$\frac{\partial\{L_{\text{md}}\}}{\partial p_k} = \frac{\partial[K_{LE}]}{\partial p_k}\{\xi_E\} + [\bar{K}_{LE}]\frac{\partial\{\xi_E\}}{\partial p_k} \tag{19}$$

where $\{\xi_E\}$ is obtained by Eq. (7) and its sensitivities by Eq. (14).

Stress by Direct Modal Approach

Stresses in finite elements are related to the grid-point displacements by

$$\{\sigma\} = [SU]\{u\} \tag{20}$$

where $[SU]$ depends on the element type, material properties, and grid locations, but not on the gage properties, which are used here as design variables (hence $\partial[SU]/\partial p_k = 0$). Application of the regular modal assumption of Eq. (3) gives

$$\{\sigma\} = [\phi_\sigma]\{\xi_E\} \tag{21}$$

where $[\phi_\sigma] = [SU][\phi_E]$ is a matrix of modal stresses that is independent of the design variables. Selected rows in $[\phi_\sigma]$ are calculated during the normal mode analysis of the baseline structure and stored in the data base.

The differentiation of Eq. (21) gives the stress sensitivities to the design variables

$$\frac{\partial\{\sigma\}}{\partial p_k} = [\phi_\sigma]\frac{\partial\{\xi_E\}}{\partial p_k} \tag{22}$$

where $\partial\{\xi_E\}/\partial p_k$ is calculated by Eq. (14).

The validity of using the regular modal assumption for calculating stresses and their sensitivities with a reasonable number of low-frequency modes is a major investigation subject in this work. It will be demonstrated in the numerical example section that, when applied to a baseline structure under quasisteady maneuver loads, the direct modal approach gives element stresses with excellent accuracy, compared to the full finite element solution. However, the stress sensitivities to design variables of local nature and the stresses of the modified structure are unacceptably wrong.

Stress by Modal Perturbations

Local structural changes of nonhomogeneous nature may cause stress redistributions that cannot be adequately expressed by Eq. (21), with a limited number of baseline stress modes in $[\phi_\sigma]$. We want to improve the accuracy of the sensitivity analysis with a minimal impact on the method efficiency.

A new development is presented below with emphasis on physical insight. The discrete-coordinate displacement vector for stress analysis of the modified structure is defined as

$$\{u_s\} = \{u_0\} + \{\Delta u\} \tag{23}$$

where $\{u_0\}$ is the elastic displacement vector of the baseline structure under the modified loads and $\{\Delta u\}$ is an approximation of the displacement changes due to forces applied by the added material on the baseline structure.

The first term in Eq. (23) is treated by the regular modal approach of Eq. (3), namely

$$\{u_0\} = [\phi_E]\{\xi_0\} \tag{24}$$

where $\{\xi_0\}$ is the solution of the generalized-coordinate equilibrium of the baseline structure under the modified MD loads.

$$[K_{EE}]\{\xi_0\} = [\phi_E]^T\{F_{\text{md}}\} \tag{25}$$

which yields, with Eqs. (6), (11), (16), and (24),

$$\{u_0\} = [\phi_E]\left([I] + \sum_{k=1}^{n_p}\Delta p_k[K_{EE}]^{-1}\frac{\partial[K_{EE}]}{\partial p_k}\right)\{\xi_E\} \tag{26}$$

where the diagonal $[K_{EE}]$ and its nondiagonal sensitivity matrices already appear in the modal data base.

The second term in Eq. (23) is the solution of the discrete-coordinate equation

$$[K]\{\Delta u\} = -\sum_{k=1}^{n_p}\Delta p_k\frac{\partial[K]}{\partial p_k}[\phi_E]\{\xi_E\} \tag{27}$$

where the right side expresses the forces applied on the baseline structure by the added material, estimated by the stiffness of the added material and the modal displacement assumption of Eq. (3). Nevertheless, these are concentrated forces at locations of structural changes that yield the local deformations needed for adequate estimations of stress redistribution. Equations (23), (26), and (27) yield

$$\{u_s\} = \left([\phi_E] \left([I] + \sum_{k=1}^{n_p} \Delta p_k [K_{EE}]^{-1} \frac{\partial [K_{EE}]}{\partial p_k} \right) + \sum_{k=1}^{n_p} \Delta p_k [\phi_P]_k \right) \{\xi_E\} \tag{28}$$

where the modal perturbation matrices $[\phi_P]_k$ are the solutions of

$$[K][\phi_P]_k = -\frac{\partial [K]}{\partial p_k} [\phi_E] \tag{29}$$

The generation of all the perturbation matrices requires n_p solutions of Eq. (29), but they all use the same decomposition of $[K]$. Since $[K]$ represents a free-free structure, it is singular. Hence, the solution requires the elimination of n_R selected statically determined coordinates by constraining the corresponding rows in $[\phi_P]_k$ to zeros.

Equation (20) with $\{u\}$ replaced by $\{u_s\}$ of Eq. (28) yields

$$\{\sigma\} = [C_\sigma]\{\xi_E\} \tag{30}$$

where

$$[C_\sigma] = [\phi_\sigma] \left([I] + \sum_{k=1}^{n_p} \Delta p_k [K_{EE}]^{-1} \frac{\partial [K_{EE}]}{\partial p_k} \right) + \sum_{k=1}^{n_p} \Delta p_k [\phi_{\sigma P}]_k$$

where

$$[\phi_{\sigma P}]_k = [SU][\phi_P]_k$$

The modal stress perturbation matrices $[\phi_{\sigma P}]_k$ are conveniently calculated for the baseline finite element by defining the right side of Eq. (29) as load subcases and calculating stresses by standard static solutions. These matrices are the additional information stored in the data base before the actual optimization starts. The only terms in Eq. (30) that change during the optimization are Δp_k. It can be observed that Eq. (30) is reduced to Eq. (21) for the baseline structure, where all $\Delta p_k = 0$.

The differentiation of Eq. (30) gives the stress sensitivities

$$\frac{\partial \{\sigma\}}{\partial p_k} = [C_\sigma] \frac{\partial \{\xi_E\}}{\partial p_k} + \frac{\partial [C_\sigma]}{\partial p_k} \{\xi_E\} \tag{31}$$

where the sensitivity matrices

$$\frac{\partial [C_\sigma]}{\partial p_k} = [\phi_\sigma][K_{EE}]^{-1} \frac{\partial [K_{EE}]}{\partial p_k} + [\phi_{\sigma P}]_k$$

are independent of p_k. The most important feature of the modal perturbation method is that, once the data base is constructed, the repeated computations during the optimization process are extremely efficient. The modal displacements and their derivatives are computed in each step by the reduced-size equations (7) and (14). Sums of the data base coefficient matrices multiplied by the updated design values Δp_k are then used to calculate stresses and their derivatives by Eqs. (30) and (31). The method is conveniently applicable to several load cases simultaneously because the generalized coordinates and the modal data base are not functions of any specific loading case. Each independent structural design variable adds a modal stress perturbation matrix to the data base, but without increasing the problem size.

Numerical Application

The main purpose of the numerical application is to demonstrate the efficiency and accuracy of the modal perturbation method and the potential advantages in using it in modal-based multidisciplinary optimization schemes. Optimization studies often involve too many aspect and technical details for a single paper. In order to focus on the main purpose with clarity and physical insight, we used a simple design case and direct optimization techniques that are easy to perceive intuitively.

The application consists on a finite element MSC/NASTRAN model of a flexible aluminum wing connected to a rigid fuselage and an all-movable horizontal stabilizer. A top view of the doublet-lattice aerodynamic model is shown in Fig. 1. The semispan length is 12 m and the wing root is at $y = 1.4\ m$. Top and side views of the wing structural parts (torsion box and aileron) are shown in Fig. 2. The wing-box structure include 16 ribs, upper and lower skins, 2 spars with caps, and 10 lines of stringers along the skins. The finite element model consists of about 600 elements and 800 degrees of freedom. The wing box was divided into five zones, each having seven independent design variables: the thickness of the skin, front spar, near spar, and ribs and the cross-sectional areas of the stringers, front-spar cap, and rear-spar cap. The baseline values of the design variables, except the spar caps, are given in Table 1.

The optimization data base was constructed for the baseline structure with 2 rigid-body modes (in heave and pitch), 40 symmetric elastic modes, and 2 control modes related to the aileron and the elevator. The data required for aeroelastic optimization without stress considerations[12] include the generalized stiffness and mass matrices, their derivatives with respect to the 35 design variables, and the generalized linear aerodynamic matrices (steady and unsteady). The matrices added for stress considerations are the baseline modal stress matrix $[\phi_\sigma]$ and the 35 modal stress perturbation matrices $[\phi_{\sigma P}]_k$ in Eqs. (30) and (31). All the modal results shown in this section were calculated with this data base without returning to the finite element model. The numerical errors indicated below for the modal results are relative to full discrete-coordinate MSC/NASTRAN solutions with updated design values.

The stress design is based on a single $3g$ pull-up maneuver at sea level, Mach 0.55. There are eight trim variables in $\{X_R\}$ of Eq. (9). Four variables, heave translation, heave velocity, pitch acceleration and aileron deflection, are set to zero. The heave acceleration is fixed at $\ddot{\xi}_{R_1} = 3g$ and the pitch rate is fixed at the kinematically defined $\dot{\xi}_{R_2} = 2g/V$. The two remaining trim variables, ξ_{R_2} and ξ_{C_2}, which

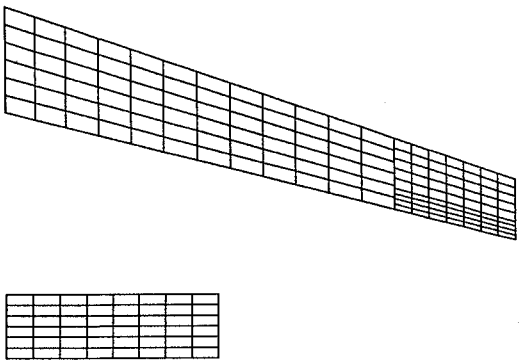

Fig. 1 Aerodynamic panel model.

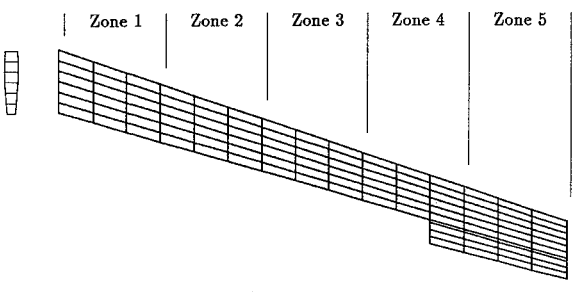

Fig. 2 Structural layout of wing.

Table 1 Initial and final values of design variables

Design variable	Value		
	Initial[a]	Final[a]	Change
rib1	5.000	0.500	−90.0%
rib2	4.000	0.500	−87.5%
rib3	3.000	0.500	−83.3%
rib4	2.000	0.500	−75.0%
rib5	1.000	0.500	−50.0%
skin1	1.500	1.703	+13.5%
skin2	1.400	2.200	+57.1%
skin2	1.300	1.800	+38.4%
skin4	1.200	1.800	+50.0%
skin5	1.100	0.996	−9.50%
fspar1	5.000	6.000	+20.0%
fspar2	4.000	4.750	+18.7%
fspar3	3.000	3.500	+16.7%
fspar4	2.000	2.300	+15.0%
fspar5	2.000	2.200	+10.0%
rspar1	5.000	6.000	+20.0%
rspar2	4.000	4.750	+18.7%
rspar3	3.000	3.500	+16.7%
rspar4	2.000	2.300	+15.0%
rspar5	2.000	2.200	+10.0%
string1	2400.0	1346.5	−43.9%
string2	2200.0	1098.6	−50.1%
string3	2000.0	864.43	−56.8%
string4	1800.0	646.60	−64.1%
string5	1600.0	472.50	−70.5%

[a]Units are mm, except for the string variables, which are mm^2.

in this case are the angle of attack α and elevator deflection δ_e, remain to be solved for by the trim equation (9). The differences between the modal trim values of the baseline structure and those calculated by the full MSC/NASTRAN static aeroelastic solution were less than 1%.

Section loads (shear, bending moment, and torsion) were calculated at several stations along the wing with percentage errors of less than 0.05%. The variations of the wing-root bending moment with percentage changes of the thicknesses of the skin and the front spar at zone 2 and the cross-sectional area of the stringers at zone 3 are shown in Fig. 3. Here and in the following figures, the different modal approach cases are marked by different isolated symbols, whereas the NASTRAN reference is marked by solid lines. It can be observed that the effects of structural variations are generally small (0.8%) for large design changes of −60% to +240%. The errors of load computations by the modal approach in this range are less than 0.1%. Large reductions of more than 90% of the skin or front-spar thicknesses cause aeroelastic divergence that is indicated by the NASTRAN solutions but not by the modal ones. Such extreme stiffness reductions should be beyond the modal approximation move limits. To check the ability of the modal approximation to predict aeroelastic divergence,[10] a new modal data base was constructed with the thickness of the front spar at zone 2 reduced by 90%, and section loads were then calculated with no perturbations. The resulting loads were practically identical to those of NASTRAN.

The von Mises stresses for typical skin, front-spar and rear-spar elements, and axial stresses for stringer elements along the wing span in the baseline structure are shown in Fig. 4. It can be observed that the modal stresses, calculated in this case by Eq. (21), are in excellent agreement with the full solution. The derivatives of these stresses with respect to the design variables were first calculated by the direct modal approach [Eq. (22)]. Typical results are the sensitivities to the skin thickness in zone 2, given in Fig. 5. The errors, especially at and near zone 2, are unacceptably large and sometimes even larger than 100%. Repeated calculations with the direct approach, this time with 55 elastic modes (instead of 40), still showed about the same errors. It is obvious that the direct approach to stresses cannot be used in our optimization scheme.

The sensitivities of the baseline stresses were also calculated with the new modal perturbation approach of Eq. (31). The derivatives with respect to the skin thickness in zone 2 are given in Fig. 6. These are the same parameters as in Fig. 5, but now the accuracy is excel-

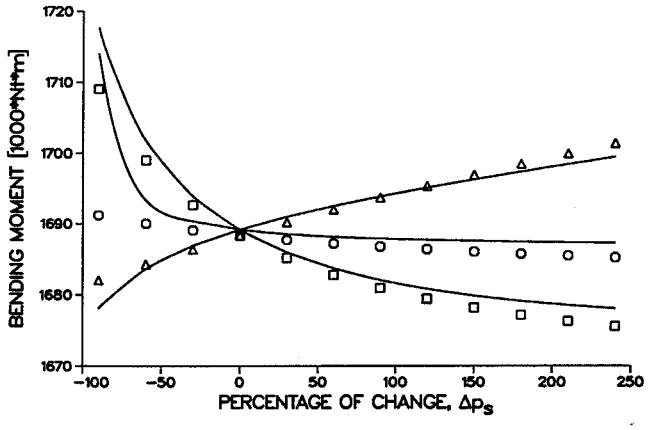

Fig. 3 Wing root bending moment vs changes in design variables; □ variation of skin2, ○ variation of fspar2, △ variation of string3, Nastran reference.

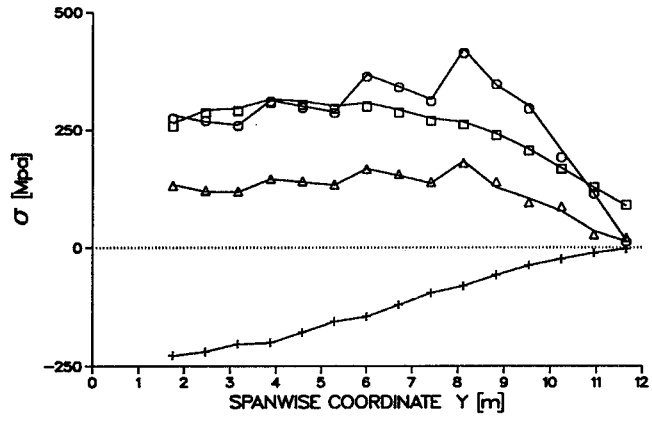

Fig. 4 Wing stress field in pull-up maneuver; □ skin elements, ○ front spar elements, △ rear spar elements, + stringers, Nastran reference.

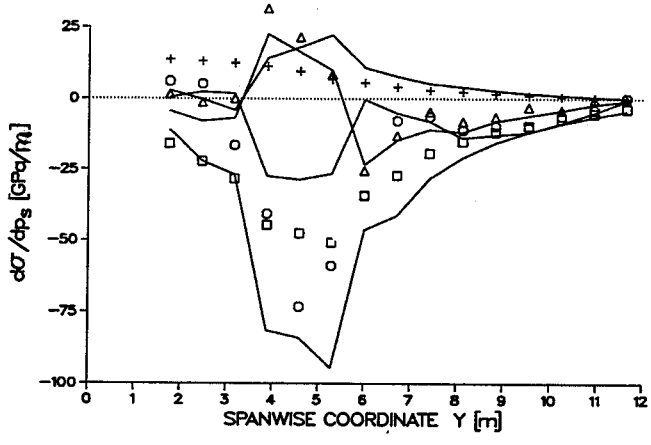

Fig. 5 Stress sensitivities to skin2: direct approach; □ skin elements, ○ front spar elements, △ rear spar elements, + stringers, Nastran reference.

lent, as good as the accuracy in calculating stresses [Fig. 4]. Other stress sensitivities (not shown) exhibited similar levels of accuracy.

The variations of von Mises stresses of an upper skin element (1212) in zone 2, a frontspar element (2202) in zone 2, and the axial stress in an upperskin stringer (4312) in zone 3, with percentage changes of the front-spar thickness in zone 2, are shown in Fig. 7. Although the effects on stresses in the skin and stringer elements are small (except when divergence is approached), the effects on stresses in the changed elements is of course large. A good agreement of Eq. (30) with NASTRAN results is shown for the stress values and their slopes at the baseline case ($\Delta p_s = 0$). At a move range of −30% +50% we still get accuracy of 10%, but larger changes exhibit diverging errors. Among many analyzed stresses, this case gave the worst accuracy. A more typical case, stresses in the same

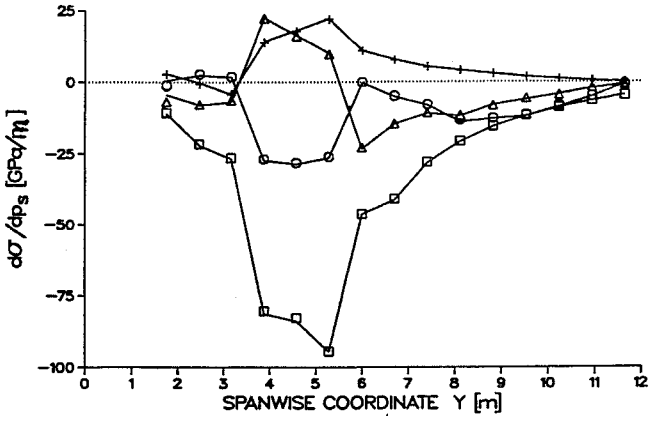

Fig. 6 Stress sensitivities to skin2: modal perturbation approach; □ skin elements, ○ front spar elements, △ rear spar elements, + stringers, Nastran reference.

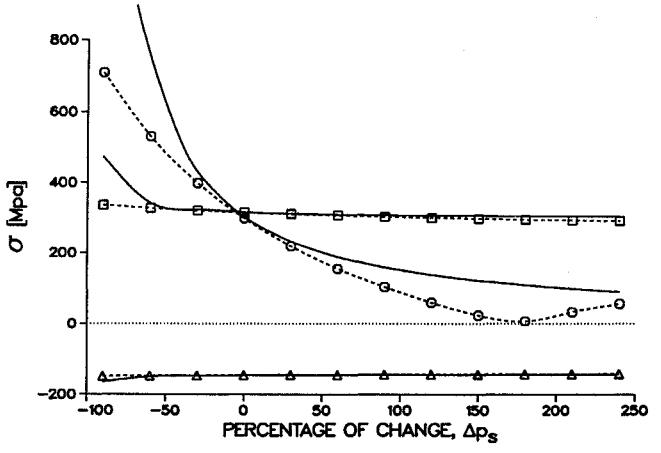

Fig. 7 Stress in various element vs percentage of change in fspar2; □ skin element 1212, ○ front spar element 2202, △ stringer 4312, Nastran reference.

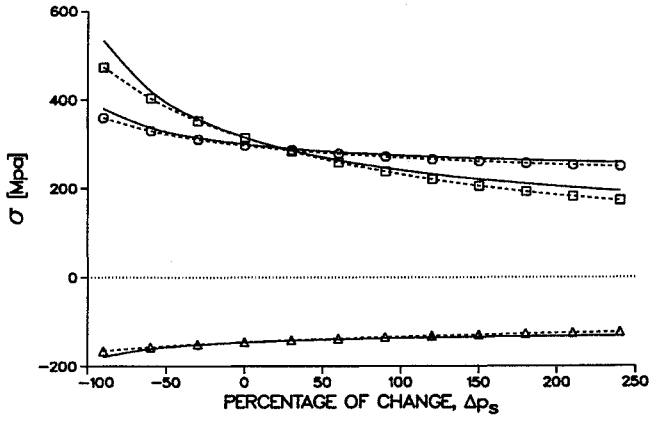

Fig. 8 Stress in various elements vs percentage of change in skin2; □ skin element 1212, ○ front spar element 2202, △ stringer 4312, Nastran reference.

elements with changes in the skin thickness in zone 2, is shown in Fig. 8. The changes now affect all the elements, and the errors are significantly lower. It should be noted that changes of a single local design variable is usually more severe than the more evenly distributed changes in typical optimization cycles.

Convergence analyses were performed to investigate the effects of the number of elastic modes taken into account. Convergence is assumed when a continued increase of the number of modes taken into account does not change the results significantly. Integral parameters such as control effectiveness and section loads needed only 10 modes to converge. Their sensitivities required up to 15 modes to converge. Element stress converged with 15 modes for the baseline structure and with 20 modes for the modified structures. The errors shown in the previous paragraphs indicate that convergence does not necessarily imply accurate results. Convergence plots (not shown) were generated up to 55 modes. A larger number of modes, even if it eventually gives more accurate results, might yield inefficient data preparation and optimization processes.

Stress considerations were added to the aeroelastic optimization scheme of Ref. 12 and a multiobjective optimization was performed with weight, stress, control effectiveness, and flutter considerations. The optimization objectives were minimal weight; flutter dynamic pressure $q_f > q_{f,\min}$, where $q_{f,\min} = 30,842\ Pa$ (20% airspeed margin); aileron effectiveness in roll, η_δ, of at least $\eta_{\min} = 0.20$ at the design point; and element stresses under limit loads of not more than $\sigma_{\lim} = 330$ MPa. These behavior constraints where satisfied by defining the weighted exponential cost function

$$f(\{\Delta p\}) = A_w W_s + \exp\left[-A_{q_f}\left(\frac{q_f}{q_{f,\min}} - 1\right)\right] + \exp\left[-A_{\eta_\delta}\left(\frac{\eta_\delta}{\eta_{\min}} - 1\right)\right] + \sum_{j=1}^{\eta_\sigma} \exp\left[-A_\sigma\left(1 - \frac{\sigma_j}{\sigma_{\lim}}\right)\right] \tag{32}$$

where W_s is the structural weight and A_w, A_{q_f}, A_{η_δ}, and A_σ are weighting coefficients. This easily differentiable cost function assigns large penalties to violations of the design requirements. A steepest descent algorithm was used to reduce the cost function without violating the prescribed move limits.

The analysis routines pass the behavior values W_s, q_f, η_δ, and σ_j and their sensitivities to the optimization routine that calculates the cost function and its derivatives with respect to the design variables. The efficient computations allow tuning of the weighting coefficients in an on-line manner. More modal-based disciplines, such as control stability margins[12] and gust response,[13] can be considered by adding the respective analysis routines, assigning objectives and weighting coefficients, and expanding the cost function accordingly. Disciplines that cannot be based on low-frequency normal modes, such as buckling, can be considered by interacting with other codes using multilevel decomposition schemes.[17]

The flutter analysis and the related sensitivity computations were performed by the state-space methods of Ref. 12. The minimum-state weighted unsteady aerodynamic approximations added 10 aerodynamic states. The stability boundary points were found by root-locus analysis with dynamic residualization of 35 of the 40 data base elastic modes.

The weight of the baseline wing was about 1700 kg. To demonstrate the coupling between the weight, flutter, and stress disciplines and to yield significant nonhomogeneous structural changes in order to check the method accuracy, the baseline cross-sectional area of the stringers was purposely increased to move the wing bending frequency closer to the torsion frequency, which caused the flutter dynamic pressure to drop to about 30% below $q_{f,\min}$. In addition, two front-spar elements violated the stress requirements, one by 10% and one by 30%. Each optimization step was aimed at reducing the cost function by 4%. The optimization process was stopped arbitrarily after 10 steps. The initial and final design gages of 25 design variables are compared in Table 1. Changes in the 10 spar-cap variables (not shown) were insignificant. Round-figure final values indicate reaching maximal allowed moves. It can be observed that the structural changes are significant and far from being homogeneous.

The changes of wing weight and selected stresses with the optimization steps are given in Figs. 9 and 10. In the first five steps, the process was focused on reducing the large penalties due to the violations of the flutter and stress margins, with a small impact on the total weight. The last five steps reduced the wing weight by about 20% while keeping the required margins. Control effectiveness values exceeded the requirements considerably throughout the process and, hence, did not affect the design significantly. NASTRAN stresses that were calculated in each step with design variables of the optimization process are also shown in Fig. 10. It can be observed that the stress errors increase as the structure deviates from the starting point. The maximal errors among all elements with high stresses are those of the front spar in Fig. 10: 2% at the starting point and 6.5% at the end.

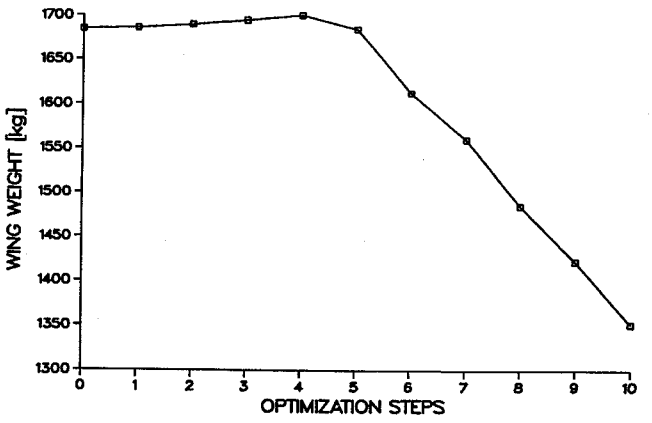

Fig. 9 Variations of wing structural weight in optimization process.

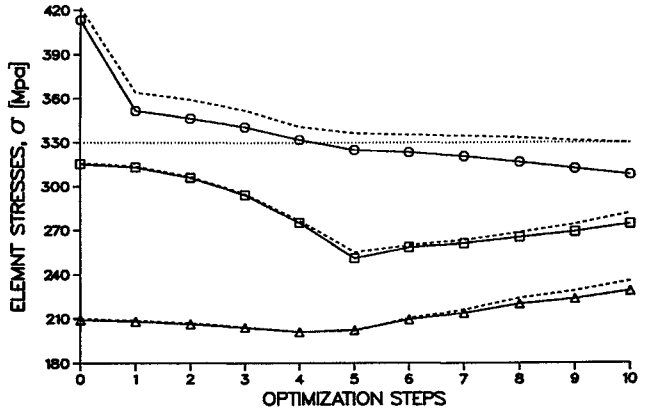

Fig. 10 Variation of stresses in various elements in optimization process; □ skin element 1212, o front spar element 2401, △ stringer Element 4151, Nastran reference.

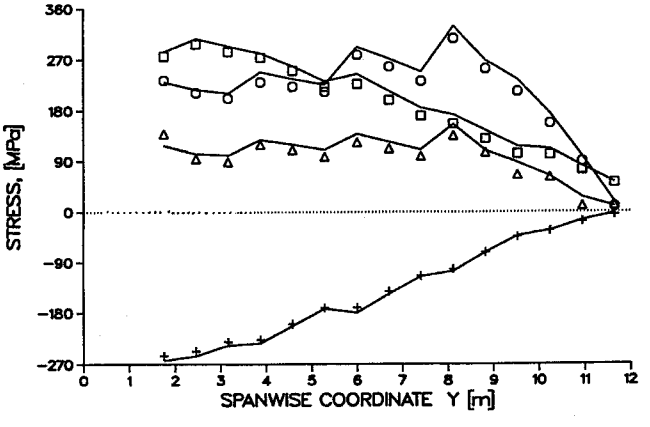

Fig. 11 Stress field in updated structure after 10 optimization steps; □ skin elements, o front spar elements, △ rear spar elements, + stringers, Nastran reference.

The stress field that was shown in Fig. 4 for the baseline structure is shown in Fig. 11 for the final design. The errors in Fig. 11 are larger, but still under 7%. The entire process was repeated with only 20 elastic modes and showed insignificant changes, in all aspects, compared with the 40-mode results.

The main advantage of the modal approach is its computation efficiency. The entire 10-step optimization process described above, after the baseline data base was prepared, took 161 CPU seconds on a DEC VAX 9000-210 mainframe. One static solution (trim, loads, and stresses), after the model was constructed, took 0.08 CPU seconds with the modal approach, compared to 29.8 CPU seconds with MSC/NASTRAN. Static solution plus sensitivity analysis with modal perturbations took 3.62 CPU seconds. The use of 20 elastic modes instead of 40 reduced the execution times of the modal methods by about 65%.

Conclusions

The presented modified formulation of static aeroelasticity provides an extremely efficient way to analyze loads and stresses in aeroelastic systems and to include them in multidisciplinary aeroservoelastic optimization schemes. It was shown that the regular data base, normally used in optimization with dynamic aeroelastic constraints, can be used for the analyses of aeroelastic trim, control effectiveness, quasisteady maneuver loads, and structural stresses under these loads as well. Sensitivity analyses can also be performed with the regular approach, but, although yielding good results for integral parameters, it yields unacceptable errors when applied to local stresses. A new method that uses modal stress perturbations was presented. The method exhibited high accuracy in calculating stresses of modified structures. The modal perturbation matrices are calculated for the baseline structure and stored in the data base for use during the optimization process. The order of the repeated static analyses, typically based on 20–40 elastic modes, remains unchanged when the new method is applied. A numerical application demonstrated that stress considerations can be added to other considerations with a marginal effect on the on-line computation time. The method is especially suitable for preliminary and early detailed design stages when the general element sizing and its effects on major stresses and on global behaviors such as flutter and interaction with the control system are of main interest.

Acknowledgment

The work presented in this paper was partially supported by NASA Grant NAGW-1708.

References

[1]Haftka, R. T., "Automated Procedure for Design of Wing Structures to Satisfy Strength and Flutter Requirements," NASA TN D-7264, July 1973.

[2]Wilkinson, K., Lerner, E., and Taylor, R. F., "Practical Design of Minimum-Weight Aircraft Structure for Strength and Flutter Requirements," *Journal of Aircraft*, Vol. 13, No. 8, 1976, pp. 614–624.

[3]Neill, D. J., Johnson, E. H., and Confield, R., "ASTROS—A Multidisciplinary Automated Structural Design Tool," *Journal of Aircraft*, Vol. 27, No. 12, 1990, pp. 1021–1027.

[4]Climent H., and Johnson, E. H., "Aeroelastic Optimization Using MSC/NASTRAN," *Proceedings of the International Forum on Aeroelasticity and Structural Dynamics*, Strasbourg, France, May 1993, pp. 1097–1116.

[5]Bisplinghoff, R. L., Ashley, H., and Halfman, R. L., "Aeroelasticity," Addison-Wesley, Reading, MA, 1955.

[6]Livne, E., Schmit, L. A., and Friedmann, P. P., "Integrated Structure/Control/Aerodynamic Synthesis of Actively Controlled Composite Wings," *Journal of Aircraft*, Vol. 30, No. 3, 1993, pp. 387–394.

[7]Giles, G. L., "Equivalent Plate Analysis of Aircraft Wing Box Structure with General Planform Geometry," *Journal of Aircraft*, Vol. 23, No. 11, 1986, pp. 859–864.

[8]Bindolino, G., Lanz, M., Mantegazza, P., and Ricci, S., "Integrated Structural Optimization in the Preliminary Aircraft Design," *Proceedings of the Seventeenth Congress of the International Council of the Aeronautical Sciences* (Stockholm, Sweden), 1990, pp. 1366–1378.

[9]Noor, A. K., and Lowder, H. E., "Approximate Techniques of Structural Reanalysis," *Computer and Structures*, Vol. 4, No. 4, 1974, pp. 801–812.

[10]Karpel, M., and Sheena, Z., "Static Aeroelastic Analysis Using Aircraft Vibration Modes," *Proceedings of the Second International Symposium on Aeroelasticity and Structural Dynamics* (Aachen, Germany), 1985, pp. 229–232.

[11]Sheena, Z., and Karpel, M., "Structural Optimization for Aeroelastic Control Effectiveness," *Journal of Aircraft*, Vol. 26, No. 5, 1989, pp. 493–495.

[12]Karpel, M., "Multidisciplinary Optimization of Aeroservoelastic System Using Reduced Size Models," *Journal of Aircraft*, Vol. 29, No. 5, 1992, pp. 939–946.

[13]Zole, A., and Karpel, M., "Continuous Gust Response and Sensitivity Derivatives Using State-Space Models," *Journal of Aircraft*, Vol. 31, No. 5, 1994, pp. 1212–1214.

[14]Haftka, R. T., Gurdal, Z., and Kamat, M. P., *Elements of Structural Optimization*, 2nd ed. Kluwer Academic, Dordrecht, The Netherlands, 1990.

[15]D'Vari, R., and Baker, M., "A Static and Dynamic Aeroelastic Loads and Sensitivity Analysis for Structural Loads Optimization and Its Application to Transport Aircraft," AIAA Paper 93-1643, April 1993.

[16]Karpel, M., and Presente, E., "Structural Dynamic Loads in Response to Impulsive Excitation," *Proceedings of the International Forum on Aeroelasticity and Structural Dynamics* (Strasbourg, France), 1993, pp. 1059–1176.

[17]Sobieszczanski-Sobieski, J., "Sensitivity Analysis and Multidisciplinary Optimization for Aircraft Design: Recent Advances and Results," *Journal of Aircraft*, Vol. 27, No. 12, 1990, pp. 993–1001.